FLUORESCENT EMISSION ANGIOGRAPHY

By

WILLIAM S. BICE, JR.

A DISSERTATION PRESENTED TO THE GRADUATE SCHOOL
OF THE UNIVERSITY OF FLORIDA IN
PARTIAL FULFILLMENT OF THE REQUIREMENTS
FOR THE DEGREE DOCTOR OF PHILOSOPHY

UNIVERSITY OF FLORIDA

1985

For Pat and the boys,

Billy, Greg & the Bean

ACKNOWLEDGMENTS

There are many people to whom I am indebted for the ability to accomplish this work. Let me begin with my family which supported me through the tantrums as well as the ecstasy. Although their contributions are not directly evident, my wife's and children's sacrifices were beyond the call of duty and the enabling forces behind the scenes.

My mentor for this dissertation was Dr. Alan M. Jacobs. I sincerely appreciate the grand amounts of time he devoted. He was as willing to get his hands dirty as to send me staggering off with a wealth of ideas and information. The work would never have progressed without him.

Many people provided me with equipment: Dr. Carl Pepine, most of the medical equipment as well as a place to work for about 8 months; Dr. John Wethington and the Nuclear Engineering Sciences Department, the x-ray equipment, the detection equipment and a place to work the rest of the time; Dr. Edward Carroll, a pulser; Dr. John Cox, the digital motor and driver; Dr. Larry Fitzgerald, x-ray film, a pinhole camera and an ionization chamber; and Dr. Genevieve Roessler, a second ADC. Kathy Thomas obtained a detector with a side looking mount.

I am appreciative of those who gave their time to help me: Linda Thompson who performed the surgery, Ken Fawcett for his electrical expertise;, Henry Gogun and Professor Glen Schoessow who aided with

the machining, and Dr. Robert Devine who insisted the square artery assumption was a good start. Lois Carroll typed all of the manuscripts associated with this work.

These are of course only some of the people who made contributions to this work. Numerous others gave time, equipment, and ideas and although I cannot thank each one in writing, I promise not to scrounge from them anymore.

My monetary support for this period has been provided by the United States Army.

TABLE OF CONTENTS

LIST OF TABLES

LIST OF FIGURES

Abstract of Dissertation Presented to the Graduate School
of the University of Florida in Partial Fulfillment of the
Requirements for the Degree of Doctor of Philosophy

FLUORESCENT EMISSION ANGIOGRAPHY

By

William S. Bice, Jr.

August 1985

Chairman: Alan M. Jacobs
Major Department: Nuclear Engineering Sciences

To reduce observer variability in the diagnosis of atherosclerosis, a new method of arteriography has been developed. Fluorescent emission angiography, an inherently three-dimensional technique, is independent of the angle of incidence--unlike conventional transmission techniques. Analytical and experimental results show it to be a fast, precise method of quantitatively measuring the arterial lumen and a sensitive measure of flow rate. Because measurement via fluorescence requires one to ten percent of the concentration of iodinated contrast agent that is conventionally used, smaller catheters and lower injection rates promise fewer complications. X-ray dose to patients and angiographic personnel can be lowered by one to three orders of magnitude. The methods developed and presented here have resulted in the ability to image with 0.3 mm resolution with an

uncertainty of less than 3 percent. Correlation with conventional transmission results *in vivo* is extremely high ($r = 0.98$) in cases where the arterial cross section is almost circular and conventional methods are not suspect. Improvements in equipment promise a reduction of the attainable resolution to 0.1 mm.

CHAPTER ONE
INTRODUCTION

Current Methods

Selective coronary angiography is the preferred method of diagnosing the extent of atherosclerotic disease in coronary arteries. Because the lesions are often eccentric, multiplanar views of the same arterial section are often generated in order to provide the angiographer a clearer image of the 3-dimensional character of stenoses. Despite its highly subjective nature [Zi76], attempted quantification of the blockage via angiography is often the prime factor upon which therapeutic decisions are based. Computerized edge detection and analysis [Kr81, Br83] and videodensitometry [Ni84] have been used to address this subjectivity.

This work demonstrates that x-ray fluorescence from the iodine in the artery, detected by an energy-resolving detector at an angle off the source-artery beam line, can be used to more precisely determine the degree of blockage. The fluorescence technique offers many advantages: a true 3-dimensional image requiring little or no subjective evaluation; much smaller doses of contrast agent given at slower injection rates and permitting the use of smaller catheters; orders of magnitude reduction in x-ray dose to the patient; and the ability to measure the flow rate at the site of injection.

Detection of x-ray fluorescence as a tool to quantify parameters *in vivo* is not a new concept. Original studies include work by

Kaufman et al. [Ka72, Ka73] who used iodine fluorescence induced by an x-ray source to study cardiac output. Ter-Pergosian et al. [Te71, Te72, Gr72] quantified regional cerebral blood flow using similar techniques. These techniques were quickly supplanted by radioisotopic procedures. Thyroid scanning, using iodine fluorescence from the natural elemental distribution excited by gamma rays from ^{241}Am, has been developed by Hoffer et al. [Ho68, Ho71, Ho73] and clinically tested by Thrall et al. [Th78]. Patton et al. [Pa76] have shown that fluorescence effectively discriminates between benign and malignant nodules. Similar methods have been used to measure cadmium content of the kidney by Ahlgren and Mattson [Ah81] and iodine content of the liver by Koehler et al. [Ko76].

In this work fluorescent emission is developed as an angiographic method, experimentally verified, and extended to demonstrate the feasibility of performing coronary angiography. Theoretical models are investigated in terms of their validity. Laboratory verification on a series of models ranging from simple tubes imaged in air to canine carotid arteries imaged in vivo is presented with the goal of coronary angiography, with its attendant complications, as the primary motivation.

Theory

X-ray fluorescence occurs when an atom which has undergone emission of a photoelectric electron de-excites. Because the energy span between shells is (for the purposes of this work) fixed, the energies of the emitted photons are characteristic of the type of atom. Nature dictates the most probable fluorescence occurs at the K_α energy--the energy difference between the K shell and L shell--when the excitation

energy is great enough to eject a K-shell electron. Several processes compete with production of K_α fluorescence: filling of the empty K shell by other than L-shell electrons, photoelectric absorption by other than K-shell electrons, and de-excitation via the production of Auger electrons. Despite this, an x ray of 33.2 keV or greater energy which is photoelectrically absorbed in an iodine atom produces a K_α fluorescence (28.5 keV) about 58% of the time. Appendix A roughly outlines, using propagation of error analysis, the impetus for fluorescent imaging: the technique betters transmission angiography in terms of x-ray dose required to produce an image of the lumen with the added advantage of providing a quantified, 3-dimensional picture at significantly lower doses of contrast agent.

Post catheterization iodinated contrast agent is injected so as to achieve a uniformly mixed solution at the site to be investigated. Figure 1-1 shows two collimation modes in which the incident x-ray beam is shaped and articulated to give different source volumes for the fluorescence. The dimensional nature of the technique is also highlighted because the fluorescent response is a function of all of the iodine atoms in the beam, the result is a volume-averaged fluorescence with spatial resolution limited by the size of the incident beam. The information provided is inherently 3-dimensional--as the beam is scanned along the artery the resultant volumetric data is stacked to provide a picture of the arterial lumen. A detector placed off the source beam line detects Compton scatter as well as iodine fluorescence; energy resolution is used to distinguish between the two. Compton noise is reduced by choosing a detection angle that exploits the isotropic nature of the fluorescence and by shielding the

Figure 1-1. Fluorescent scan beam collimation modes. The two beam modes, (a) the fan beam and (b) the pencil beam, are used to create different source volumes for fluorescence. The fan beam is swept along the long axis of the artery while the pencil beam is swept perpendicular to the long axis.

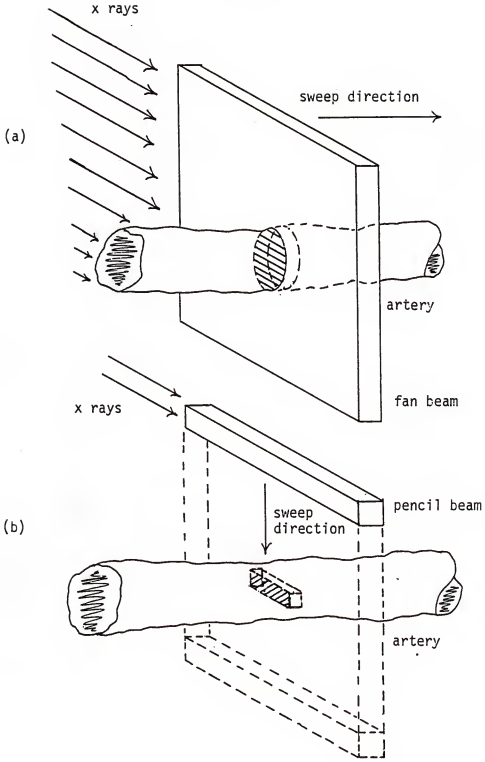
x rays
(a)
sweep direction
artery
fan beam
x rays
(b)
sweep
direction
pencil beam
artery

detector so that the entrance and exit paths of the illuminating beam are not fully viewed.

The fluorescent signal strength is indicative of the quantity of iodine illuminated by the beam. The analytical portion of this work is devoted to relating the size of the signal to volume of the arterial lumen and the rate of flow through the artery. The experimental portion is concerned with verifying the analytical results. The success achieved with available equipment strongly motivates extension to coronary angiography.

CHAPTER TWO
ANALYSIS

Analytical Goals

The analytical efforts fall into two categories, (1) modeling the fluorescent response of a contrast-filled artery considering the effects of attenuation and self shielding and (2) studying the effect of surrounding tissues in terms of the Compton scatter produced. The modeling begins with an assumption of a cylindrical lumen and examines a series of approximations to develop a model which is calculationally easy but still sufficiently describes the fluorescent response so as to remain useful. Termed the square artery assumption (SAA), this model is analytically compared to conventional transmission techniques for eccentric lumen shapes.

The effects of Compton scatter from surrounding tissue are twofold: Compton photons may fall on the arterial lumen and subsequently cause fluorescence--this is termed false signal--or the Compton photons may fall directly on the detector--this is termed Compton noise. While the experimental techniques employed were chosen to address and eliminate these effects, the magnitude of the hindrance and how the experimental design affects the experiment are proper analytical questions.

Circular Cross Sections

For the coordinate system illustrated in Figure 2-1, an arterial lumen with circular cross section generates the fluorescent signal, S, at a detector located at right angles from the source beam line.

Figure 2-1. Calculational coordinate system. The x-axis is the longitudinal axis of the artery. For an artery of radius, r, the SAA assumes a square of side, $\alpha = \sqrt{\pi}r$.

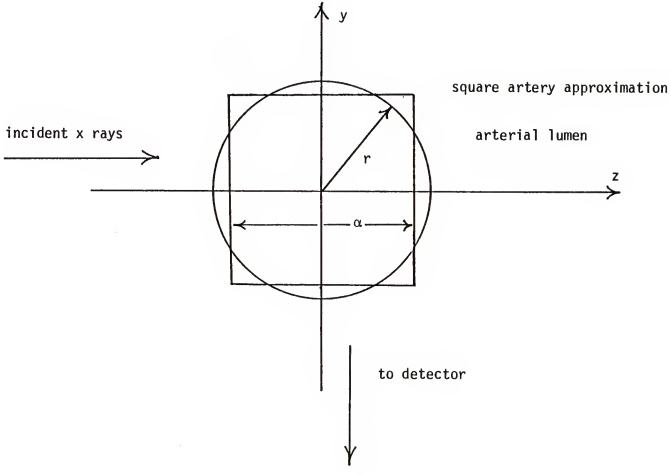
y
square artery approximation
incident x rays
arterial lumen
r
z
α
to detector

$$S = K \int_E N\tau_c(E)\phi_I(E) \int_{-r}^{r} e^{-\mu(E')y-\mu(E)(r^2-y^2)^{1/2}} \int_{-Z_o}^{Z_o} e^{-\mu(E)z-\mu(E)(r^2-z^2)^{1/2}} \, dz dy dE \quad [s^{-1}]$$

where $K = \dfrac{t_x \varepsilon A_{det}}{4\pi d^2}$ [cm]

where t_x = the thickness of the beam slice [cm]

ε = the detector efficiency (about 1.0) [ ]

A_{det} = the area of the detector face (assumed normal to the scattering volume) [cm^2]

d = the distance from the scattering volume to the detector face (assumed >> r) [cm]

r = the arterial radius [cm]

z_o = $z_o(y) = (r^2-y^2)^{1/2}$ [cm]

N = the density of iodine atoms [cm^{-3}]

$\tau_c(E)$ = the iodine photoelectric cross section corrected for probability of K emission [cm^2]

$$\tau_c(E) = \begin{cases} 0 & E < 33.2 \text{ keV} \\ .58\tau(E) & E > 33.2 \text{ keV} \end{cases}$$

$\phi_I(E)$ = the flux of photons incident on the artery [$cm^{-2}s^{-1}keV^{-1}$]

$\mu(E)$ = $\mu(E,N)$ = the total linear attenuation coefficient [cm^{-1}]

E = the incident photon energy [keV]

E' = the $K\alpha$ emission energy, 28.5 keV.

The Square Artery Approximation

Although the integral is resolvable numerically, a series of reasonable assumptions leads to the useful square artery approximation [SAA].

$$S = K_a K_g pA \frac{[1-e^{-\mu'\alpha}][1 - e^{-\bar{\mu}\alpha}]}{\mu'\bar{\mu}}$$

where

K_a = a constant which allows for attenuation of the incoming and outgoing beams [ ]

K_g = a constant which allows for geometrical losses from source to artery and artery to detector [ ]

p = the fraction of contrast agent in the illuminated volume [ ]

A = the x-ray source time integrated current [cm^{-2}]

μ' = (E',p) = the linear attenuation coefficient at the K emission energy [cm^{-1}]

$\bar{\mu} = \overline{\mu(E,p)}$ = the flux weighted linear attenuation coefficient at the surface of the artery [cm^{-1}]

α = the side of a square that has the same area as the circular lumen cross section; $\alpha^2 = \pi r^2$ [cm].

Appendix B details the assumptions and steps required to make the SAA. As the optical paths become very small ($\bar{\mu}\alpha \ll 1$ and $\mu'\alpha \ll 1$) the expression for the signal reduces, as expected, to

$$S \sim pr^2.$$

Flow Rate Measurement

The flow past the catheter is measured by injecting the contrast agent at different rates. In each case the signal via the SAA is

$$S_i = K_a K_g p_i A_i \frac{[1-e^{-\bar{\mu}_i \alpha}][1-e^{-\mu_i \alpha}]}{\bar{\mu}_i \mu_i'}$$

where the subscript, i, denotes the i^{th} flow rate. Conservation of mass implies

$$p_i = \frac{I_i}{I_i + F}$$

where I_i = the injection rate for the i^{th} measurement [ml s^{-1}]

F = the flow rate of blood in the artery past the catheter [ml s^{-1}].

Using the least-squares fitting procedure described in Appendix C the flow may be measured by the shape of the curve generated by different injection rates plotted versus the fluorescent responses.

Spectral Parameters

The parameters in the above formulation are highly dependent upon the incident x-ray spectrum. Published spectra [Bi 79] can be coupled with cross sectional data [Hu69] to give the following relationships at 5 centimeters depth.

$$\bar{\mu}_i = \bar{\gamma} p_i + \bar{\delta}$$

$$\mu_i = \gamma p_i + \delta'$$

$$N\bar{T}_i = \bar{\beta} p_i$$

where $\bar{\gamma} = 4.80$, $\bar{\delta} = .310$, $\gamma' = 3.19$, $\delta' = .394$, and $\bar{\beta} = 2.52$ for Renographin-76® diluted in water to fraction, p_i.

Spatial Spread

Although the high resolution, on the order of a tenth of a millimeter, usually precludes correction for non-uniformity across the beam, in some of the present work a therapeutic x-ray source was used.

Because of the large focal spot, the beam width at the artery was about 4 millimeters. In this case the one-dimensional point spread function, P(x), was measured so that the comparison between fluorescent emission and actual diameters could be made in terms of the detector response, i.e., following the convolution,

$$S(x) = \int_{-\infty}^{\infty} P(x-x')R(x')dx'$$

where

P(x-x') is the measured point spread function,

R(x) is the diameter measured via angiography, and

S(x) is the diameter as seen by the detector due to the spread of the illuminating beam, assuming circular cross sections.

Computer Models

Various computer models were used to test the validity of analytical simplifications. Ranging from Monte Carlo transport to single-point, single-scatter analysis the computer models established the utility of the various analytic tools. A listing of the computer programs and a brief synopsis of their functions is contained in Appendix D.

Fluorescent Signal

In order to calculate the fluorescent response of a detector to a cylindrical arterial model, a 3-dimensional Monte Carlo code, PHOTRANS, was written. The program uses splitting and Russian roulette as a means of reducing the required number of particle histories. Emission, scattering and absorption sampling routines follow those outlined by Carter and Cashwell [Ca76] with the exception

of an iterative procedure developed to sample the Klein-Nishina relation. Random numbers were generated via a multiplicative congruential method.

The program, FSIG, was written to calculate the fluorescent signal generated for any lumen shape. The code assumes single-scatter interactions with incident flux correction; that is, scattering results only in the loss of the photon and attenuation follows a simple exponential model. Figure 2-2 shows the error bounds in measurement introduced by irregularly shaped lumina. The large optical paths were purposely chosen for this analysis to highlight the validity of the SAA as a reconstructive method. Perpendicular projections with the attendant changes in self attenuation give the bounds for the fluorescent response error. Also shown is the calculated error bounds introduced in transmission angiography given the best and worst projections and no edge unsharpness.

Figure 2-3 shows the calculated signals for a cylindrical arterial lumen 4.67 mm in diameter at various percentages of contrast agent. The four methods of calculation (Monte Carlo, single-scatter, SAA with variable cross sections, and SAA with constant cross sections) are in good agreement throughout the entire range of contrast agent percentage (about 3.6 optical paths). Because the approximation of very small optical paths quickly breaks down, the linear model ($S \sim pr^2$) can rarely be used. The large uncertainty in the Monte Carlo values is due to the small number of particle histories. Later in this work experimental measurements are combined with the mathematical models. The goal, based upon these results, is to work at low concentrations so that the optical path is less than one when using the SAA

Figure 2-2. Errors introduced by eccentrically shaped lumina. Shaded areas are stenoses. Lumina (a) - (c) are ellipses of increasing eccentricity, (d) - (h) are crescent-shaped and of decreasing ratio of circumference to area. All cross-sectional areas are equal to that of a 4.67 mm artery and all are filled with 5% concentration of Renografin-76®. Upper values are minimum and maximum projection errors introduced by transmission angiography. Lower values are minimum and maximum projection errors introduced by fluorescent emission angiography.

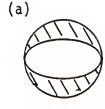

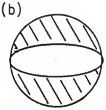

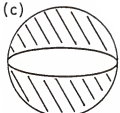

Conventional	-50% to +200%	-67% to +300%	-75% to +400%
Fluorescence	-1% to -2%	-1% to -3%	-3% to -5%

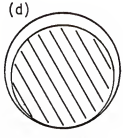

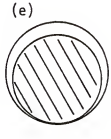

Conventional	+460%	+370%	+290%
Fluorescence	+4% to +5%	+5% to +6%	+4% to +5%

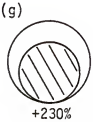

Conventional	+230%	+170%
Fluorescence	+3% to +4%	+2% to +3%

Figure 2-3. Calculated response functions for a 4.67 mm artery at different concentrations of contrast agent. The five models shown are (a) linear; (b) single scatter, circular artery; (c) square artery assumption; (d) square artery assumption with flux weighted cross sections (SAA); and (e) Monte Carlo, circular artery. Because the number of fluorescent counts depends upon geometric and attenuation factors the ordinate in this and subsequent, similar figures has arbitrary units.

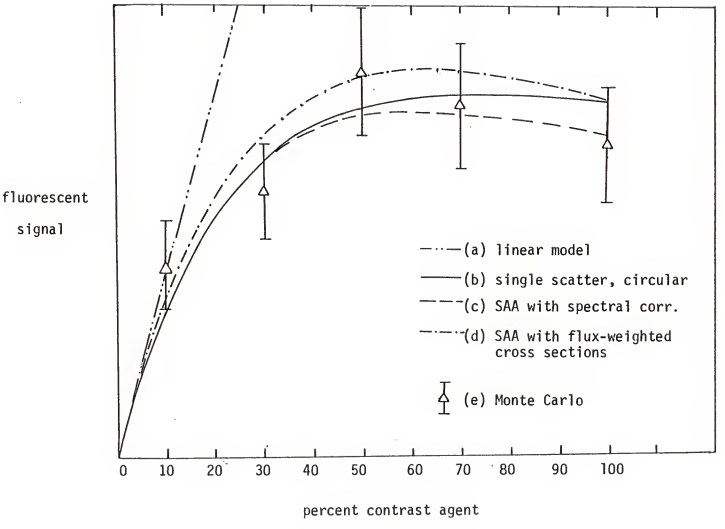
fluorescent
signal
(a) linear model
(b) single scatter, circular
(c) SAA with spectral corr.
(d) SAA with flux-weighted cross sections
(e) Monte Carlo
0
10
20
30
40
50
60
70
80
90
100
percent contrast agent

to reconstruct the lumen cross-sectional area. This arbitrarily imposed limit was designed to prevent the introduction of more than 5% error due to the use of the SAA.

Compton Effects

A single-scatter code, CSIG, similar to FSIG was written to determine the extent of the false signal generated by Compton spreading of the illuminating beam. Attenuation followed a simple exponential model and the Klein-Nishina formula is used to determine the Compton scatter cross section. The analysis is a worst-case in that a full artery is assumed on either side of the imaged volume and the Compton-scattered photons are produced in 10 centimeters of surrounding full-density tissue. As illustrated in Figure 2-4, the spread function shows an enhancing of the edges due to the large solid angle subtended and the lack of attenuation. The resultant false signal may of course be normalized out, but a loss of resolution accompanies an increase in overlying or underlying tissues. Deconvolution may be required for very precise work at depth.

Table 2-1 demonstrates the need for the energy resolving capability of the detector and a shield to reduce some of the Compton noise from the entrance and exit paths of the illuminating beam. Reducing the shielded view, or illuminated tissue seen by the detector, reduces direct Compton scatter. It should be noted that the noise in the system is not the Compton photons, but the uncertainty in eliminating the Compton spectrum from the fluorescent peak. Because a subtraction method is used, the noise in detection is related to the square root of the sum of the Compton signal and the total signal. If

Figure 2-4. Compton spread of the fluorescent signal. Shown are the effects of 5 cm of entrance and 5 cm of exit tissue on the fluorescent response at the detector for a 4.67 mm diameter artery. Area (a) shows the "true" fluorescence from the incident beam. Area (b) shows the "false" fluorescence due to Compton scatter from the surrounding tissue.

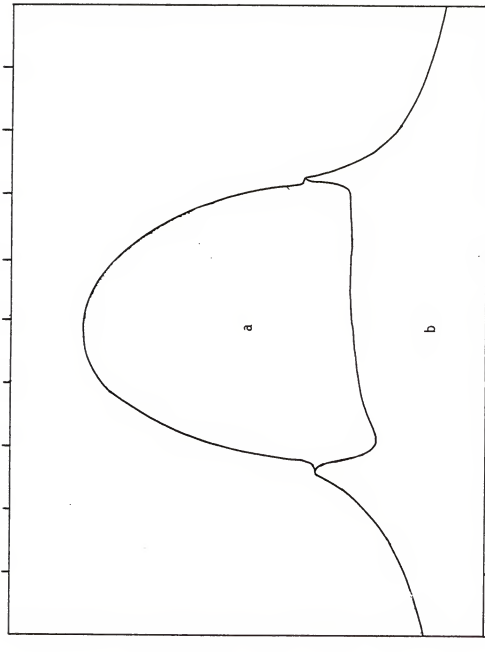
fluorescent signal
a
b
0
0.1
0.2
0.3
0.4
0.5
0.6
0.7
0.8
0.9
1.0
position (cm)

Table 2-1

Effects of Detector Energy Resolution and Shielded View for a $(0.1)^3$ mm^3 Volume Shielded by a 4 mm Diameter Artery

Window	Shielded View	Fluorescent/Compton Counts
26-33 keV	20 cm	.016
26-33 keV	1 cm	.050
27-29 keV	20 cm	.089
27-29 keV	1 cm	.294

the fluorescence were the result of a simple subtraction, the total signal (T) minus Compton signal (C), the quantum uncertainty could be written, $\sqrt{T+C}$. Thus minimizing the Compton noise is important in terms of the validity of the results.

CHAPTER THREE
EXPERIMENT

Experimental Goals

As with the analytical efforts, the experimental work concentrated on the validity of the mathematical response models and removing the effects of Compton noise. Experimental models were chosen accordingly, ranging from simple tubes suspended in air to a thorax model where Compton and attenuation effects were pronounced. Finally an *in vivo* model, a catheterized canine carotid artery, was imaged to demonstrate the utility and validity of the fluorescence technique.

Of particular interest was the equipment used. Because no fluorescent imaging system existed, one had to be constructed using available equipment. Availability determined geometry, imaging parameters, and, eventually error bounds on the results. Still, the technique works, and works well.

Geometry and Methods

A typical experimental arrangement is shown in Figure 3-1. The illuminating beam from a standard x-ray generator is highly collimated to provide the required spatial resolution at the artery. As the beam passes through the body, and the artery filled with iodinated contrast agent, a semiconductor detector placed at 90° from the beam line

Figure 3-1. A typical experimental arrangement. (a) Geometric configuration showing (1) x-ray source, (2) collimator, (3) artery, (4) shield, (5) detector, and (6) image intensifier. (b) Typical scatter spectrum. Note the spectral regions: (1) fluorescence peaks, (2) escape peak, (3) Compton noise, and (4) multiple counts. The Compton spectum separation line (5) is a 20-point second-order least-square error fit.

(a)

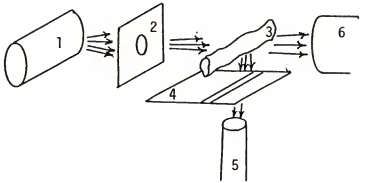

(b)

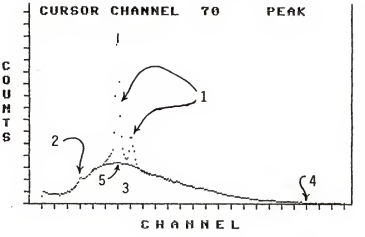

receives Compton scatter and fluorescent x rays. The Compton photons are reduced by a shield placed between the subject and the detector so that the detector sees only about a centimeter of tissue on either side of the artery. The signal from the detector is amplified and passed to a multichannel analyzer where the spectrum is sorted by energy groups and stored. The collected spectrum is then sent to a microcomputer where the analysis to separate out the fluorescence and convert the iodine counts to meaningful values is performed. The Compton continuum is subtracted from the total signal by establishing the bottom of the peak by hand and using ten points on either side of the upper and lower bounds to perform a 20-point, least-squares fit using a second-order-polynomial.

For purposes of alignment the collimator may be moved out of the beam to allow the projection image to be viewed on an image intensifier system. Transmission angiograms are produced by placing films between the subject and image intensifier in this uncollimated mode.

Equipment

The four x-ray machines used in this work were operated at 80 kVp to place the spectral peak just above the K-edge of iodine. Although some fine adjustment might have been made based upon the artery's optical depth, standardization dictated maintaining this value. Almost invariably the signal would drop with a change of 10 kVp in either direction.

The three diagnostic machines used provided the ability to image quickly and with very high resolution--due to the high currents and small focal spots available. The limiting factor became x-ray tube

heating: as the exposure time mounted the tube became more inefficient. This was primarily due to the age of the equipment. Detector dead time was also of concern, but, for the typical spectrum collected, no major dead time problems were noted until well past 200,000 counts/sec.

A therapeutic x-ray machine was also used to perform fluorescent emission angiography. While speed and resolution were sacrificed, stability was of no concern. Collection times changed from tenths of seconds to tens of seconds and the resolution attainable at the artery went from a few tenths of a millimeter to almost four millimeters. Nevertheless, exposure history had little or no effect on the output flux.

An adjustable collimator was built by milling the ends of four lead slabs and mounting them in abutting pairs on a brass sheet with a hole drilled in the middle. The collimator was then mounted on an x-y positioner driven up and down by a variable speed direct current motor and back and forth by a digital stepping motor. The collimating system is shown in Figure 3-2.

The detector was intrinsic germanium reverse biased to -1500 volts. Cooled by liquid nitrogen, the detector drove an integrally-mounted preamplifier which, in turn, drove an amplifier with a gain setting of about 150. From there the signal was sent over 30 feet of coaxial cable to a multichannel analyzer where the pulses were stored into 256 channels of a 4096-channel analog-to-digital converter. Because the dewar-cold finger configuration only allowed an upward-looking mount, the angle chosen to minimize the effect of Compton scatter

Figure 3-2. The collimation system. (a) Initial collimator, (b) abutting 1/16-inch lead slabs, (c) brass mounting plate, (d) digital stepping motor (left-right movement), and (e) 12-Volt DC variable speed motor (up-down movement).


a
b
c
b
d
e

in these experiments was always 90 degrees. This was fortunate in that the Compton cross section is also a minimum in this direction.

A schematic of the simple interface built to connect the output port of the multichannel analyzer to the input port of the microcomputer is shown in Figure 3-3. Also shown is the translator formula to convert from multichannel analyzer values to the microcomputer ASCII. Various computer programs to retrieve and interpret the data are described in Appendix D.

The pumping system built to maintain constant flow through the test section via constant pressure was constructed by maintaining a constant fill level on a reservoir mounted 6 feet, 2 inches above the subject table and adjusting the flow rate by means of an in-line valve. An overflow outlet allowed continual feed of local tap water. Variation in rate was less than 1 ml/min over a 30 minute period.

Variable speed injection was achieved via the system illustrated in Figure 3-4. While various combinations of catheter sizes, dilution of injection solution, and injection speed were tried, results indicated that thorough mixing is the sole criterion for fluorescence measurement validity. For models where this was difficult to achieve (small catheters in large diameter smooth-walled tubing) a turbulence inducer such as a balloon catheter or screen was used distal to the injection site to insure thorough mixing.

In experiments conducted with the therapy machine, an image intensifier powered by a nearby diagnostic unit was mounted to allow transmission fluoroscopy. This proved a great aid in alignment. A television camera was introduced into the mirror viewing system in order that the fluoroscopic image could be remotely viewed. This system is shown in Figure 3-5.

Figure 3-3. Interface between the computer and the multichannel analyzer. The line of code (BASIC) is used to translate from the MCA to the computer ASCII.

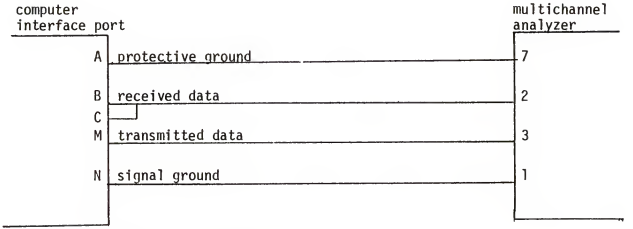

· AB%(I) = INT((255-B%(I))/2)

Figure 3-4. Harvard® injection pump. (a) 60-cc syringe and (b) 7F NIH catheter.

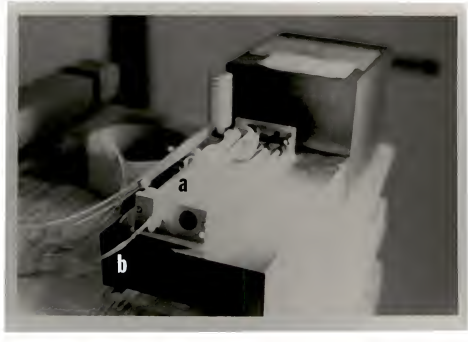
a
b

Figure 3-5. Image intensifier system. (a) Siemens® diagnostic unit image intensifier, (b) video camera, and (c) motor driven table.


a
b
c

Figure 3-6 shows the shield movement system. The two electric motors drove the slide-mounted lead sheets apart-and-together and backward-and-forward. The alignment procedure consisted of narrowing the gap between the two plates and then moving this slit along the beam path until the strongest fluorescent signal was recorded. The shield plates were then opened until the fluorescence no longer increased along the scan path. Infrequently the subject had to be reoriented so that the artery was parallel to the shield slit. This only occurred when the gap had to be opened so wide as to preclude extracting the fluorescent signal from the Compton noise.

After catheterization the entire procedure was controlled and monitored from a shielded area. The required alignment was achieved by mounting the subject and image intensifier on motor driven tables that moved up and down. The drive mechanism is shown in Figure 3-7.

The collimator movement system, shield movement system, and infusion system were also wired to allow remote control. The operation control panel is shown in Figure 3-8. Also shown is the video monitor where the output of the image intensifier and the movement of the shield system were displayed. The ability to remotely align, monitor, and take data provided an efficiency in procedure required for the experiments in vivo.

The iodinated contrast agent used in these studies was Renografin -76® manufactured by E. R. Squibb and Sons, Inc. Each milliliter contains 660 milligrams of diatrizoate sodium. Sodium citrate is added as a buffer and edetate disodium as a sequestering agent. There are about 370 milligrams of iodine per milliliter [Sq82]. Dilution was in tap water or saline solution where appropriate.

Figure 3-6. Shield movement system. (a) 1/16-inch lead shield plates, (b) 12-Volt DC motor to drive plates apart and together, (c) reversible 60-hZ AC motor and gearing mechanism to slowly move shields back and forth together, (d) counter weights, and (e) detector.

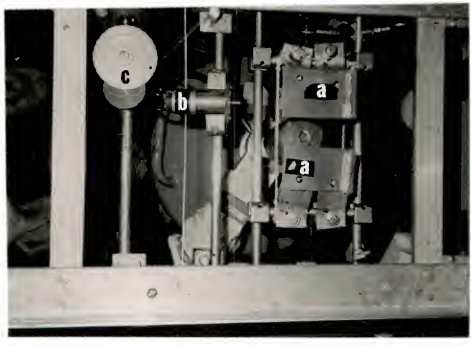
c
b
a
a

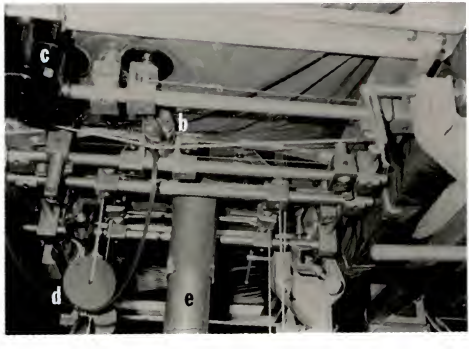
c
b
d
e

Figure 3-7. Table drive mechanism. (a) Reversible AC motor, (b) threaded table mount, and (c) drive chain.


a
b
c

Figure 3-8. Operator control panel. (a) Video monitor for image intensifier or shield movement system, (b) injection pump timer, (c) subject table up-down switch, (d) image intensifier up-down switch, (e) collimator up-down switch, (f) injection pump switch, (g) shield up-back switch, (h) shield apart-together switch, (i) DC power supply, and (j) stepping motor driver and position indicator (collimator left-right).

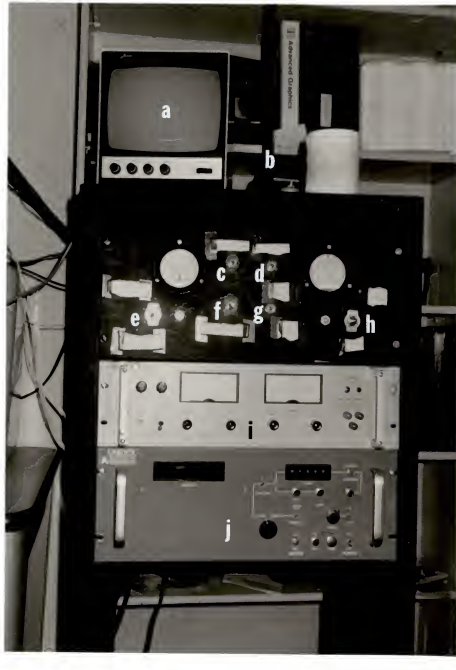
a
b
c
d
e
f
g
h
i
j

Models

The experimental models were designed to verify the validity of the mathematical calculations, measure relevant parameters, and extend the method towards clinical use. Models varied in complexity from nylon or Tygon® tubing suspended in air to tubing submerged in water behind varying thicknesses of lucite and aluminum rods. In vivo imaging of the canine carotid proved the most difficult in terms of the ability to perform the catheterization, sustain a constant flow rate, and compare the fluorescence results with the "known" arterial lumen.

The simplest models were a static solution of contrast agent diluted in water inside a tube of either nylon or Tygon®. Akin to these were models formed by drilling holes in lucite rectangular parallelepipeds and filling with dilute solutions of contrast agent. These were the models used to verify the validity of the various mathematical response formulations. The sample holder is shown in Figure 3-9.

A lucite (polymethyl methacrylate) box was constructed to perform experimentation on tubes and arteries at depth. Constructed of 1/4-inch lucite, it was used empty for some flow studies on tubing and filled with either tap water or saline solution to study tubes or arteries at depth as appropriate.

Arteries were excised canine femorals or human cadaver coronaries mounted in the lucite box. Although successfully imaged when first mounted, the pressure under which they were perfused coupled with the hostile environment tended to make them lose patency fairly quickly. The resultant flow of iodine through the arterial wall made these the least useful of the experimental studies.

Figure 3-9. Static sample holder.

The lucite box model was amended to more closely match the problems envisioned in chest imaging. This proved the most physically demanding on the fluorescence process. Additional lucite and aluminum rods were placed so as to resemble the radiographic environment encountered in chest imaging. This model is pictured in Figure 3-10.

Canine specimens were either greyhounds or mongrels. The dogs weighed between 20 and 30 kilograms. The total of five dogs used in this study were treated in accordance with guidelines established by the National Institutes of Health [Co80].

Following anesthetization via sodium pentabarbitol, the external carotid was isolated. A plastic "y" was inserted into the artery to allow imaging distal to the catheter as in selective coronary angiography. Constriction was via circular plastic occluders which slipped around the outside of the artery. Proximal to the "y" an electromagnetic flow meter probe was mounted to monitor flow rate. Sacrifice was via injection of potassium chloride.

Parameters

Parameters to be measured or verified included the x-ray machine output spectrum, the linear attenuation coefficient at the energy of fluorescence, and the point spread function on the therapeutic x-ray source. While focal spot measurements on the diagnostic machines were also made, spatial resolution at the artery was directly measured via x-ray film.

For analytical purposes, the spectra used for the diagnostic machines were those published in the literature [Bi79]. As listed in Table 3-1, agreement in the first half-value layer measurement supported this procedure. However, the second half value layer indicated

Figure 3-10. Thorax phantom. (a) One-inch lucite, (b) 1/2-inch diameter aluminum rods (2 cm center spacing), (c) 1/4-inch lucite box filled with water (artery or tube mounted 2.7 cm from front of box and 4.0 cm from bottom of box).


c
a
b

Table 3-1

Half-Value Layer Agreement for the Siemens® Diagnostic Tube

HVL	Published (Bi79)		Measured
	Surface	5.0 cm of tissue	
1st	2.42	4.11	2.30 mm Al
2nd	3.73	5.43	5.95 mm Al

a somewhat harder spectrum, so correction to 5 cm depth in tissue was always used. The parametric values, $\bar{\mu}$ and $\bar{\tau}$, derived from this spectrum withstood use in all of the models without significant change for different thicknesses of attenuating media.

The same conclusion was not valid in the case of the therapeutic machine which has a much larger focal spot and a 45 degree anode rather than a 17 degree anode. Families of static curves generated by measuring with the lucite parallelepipeds and interpreted by using a non-linear least-squares fitting procedure similar to that outlined in Appendix C (the fitting parameter was a multiplier of the weighted cross sections) indicated that the spectral weighted parameters should be multiplied by 2.08. The parameters, $\bar{\mu}$ and $\bar{\tau}$, were adjusted accordingly for the therapy beam.

The linear attenuation coefficient at the fluorescence energy, 28.5 keV, of contrast agent mixed with water was measured by generating an absorption curve for the 31.0 keV peak from a ^{133}Ba source and by using the formula

$$\mu'_{28.5} = (\mu'_{31}) \times \begin{matrix} 1.27 \text{ for contrast agent} \\ 1.13 \text{ for water} \end{matrix}$$

The empirical results in water, $\mu' = .316 + 3.23p$, compared quite favorably with the calculated results, $\mu' = .394 + 3.19p$, where p is the fraction of contrast agent. The measured value was used to interpret the fluorescent signal in further experimental work.

The point spread function of the therapeutic beam was measured by mounting a lead sheet on the static model holder (Figure 3-9) driven by attaching the digital stepping motor (Figure 3-6) and recording the

fluorescent signal from a static, tubular phantom as the lead sheet was stepped across the beam. The first derivative of the response, the point spread function, was fit using a Fourier series expansion and this expansion was used to convert from real to convolution space via the expression

$$P(x) = A_o + \sum_{i=1,10} (A_i \cos(w_i x) + B_i \sin(w_i x))$$

with $w_i = 2\pi i T$

where T is the distance from the first to last points (the wavelength) and A_i, B_i are the expansion coefficients. The response points, derivative points, and the ten-term Fourier series expansion function are shown in Figure 3-11.

Results

Shown in Figure 3-12 are the experimental data for a 4.67 millimeter diameter tube superimposed on the same mathematical models shown in Figure 2-3 for the Siemens® diagnostic unit. As expected, the larger the number of approximations the worse the fit to the data, especially at large optical path lengths. Note that the arbitrarily imposed limit of 25 percent contrast agent for this 4.67 mm diameter artery when using the square artery approximation [SAA] corresponds to about one optical path length ($\overline{\mu\alpha} + \mu'\alpha \cong 1$), well beyond the linear response region. This dramatically illustrates the utility of the SAA, as long as the one optical path length criterion is satisfied. The SAA was used in fitting the response of a series of different diameter tubes at different concentrations of contrast agent in Figure 3-13. The illustrated results were obtained on a diagnostic machine;

Figure 3-11. Point spread function measurement. (a) Fluorescent response as a 1/16-inch lead plate is moved across beam in front of a 4.67 mm nylon tube filled with 5% concentration of Renografin-76® (.0323 cm between readings). (b) Differential of curve in (a) to give the measured point spread function. The fitted curve is a ten-term Fourier series expansion.

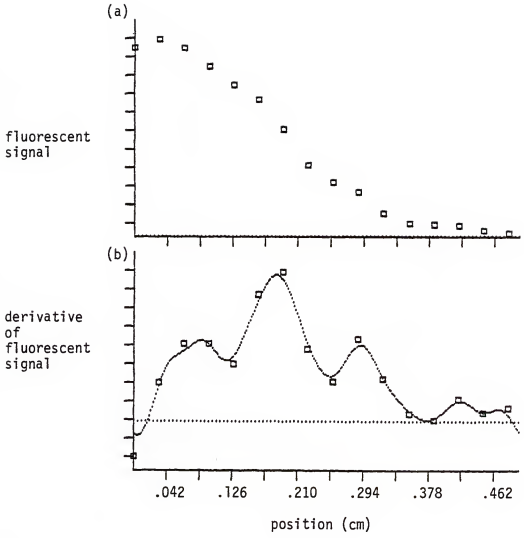
(a)
fluorescent signal
(b)
derivative of fluorescent signal
.042
.126
.210
.294
.378
.462
position (cm)

Figure 3-12. Experimental fluorescent response results compared to the mathematical models. The quantum uncertainties are smaller than the data points.

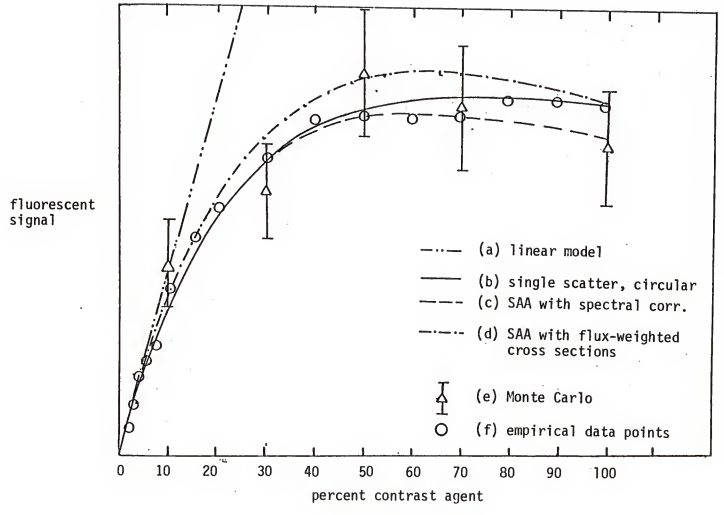
fluorescent signal
(a) linear model
(b) single scatter, circular
(c) SAA with spectral corr.
(d) SAA with flux-weighted cross sections
(e) Monte Carlo
(f) empirical data points
0
10
20
30
40
50
60
70
80
90
100
percent contrast agent

Figure 3-13. The square artery approximation model for a series of different diameter tubes at different concentration of contrast medium. The quantum uncertainties are smaller than the data points.

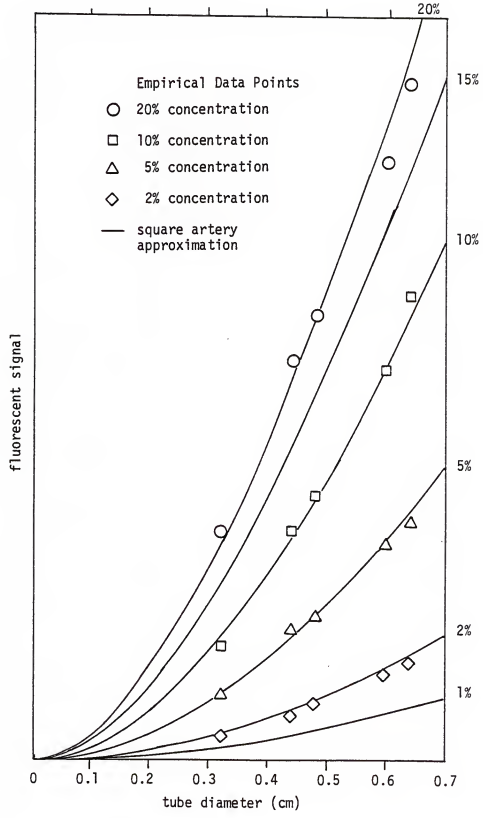
20%
15%
10%
5%
2%
1%
Empirical Data Points
20% concentration
10% concentration
5% concentration
2% concentration
square artery approximation
fluorescent signal
0
0.1
0.2
0.3
0.4
0.5
0.6
0.7
tube diameter (cm)

similar agreement was obtained on the therapeutic machine with the parallelepiped models. These results leave little doubt as to the validity of this tool when reconstructing the cross-sectional area from a fluorescent response in the fan beam mode.

Except for the additional noise, the environment in which the arterial model was placed made little difference to the technique. With the available machinery, the measurement uncertainty in any single measurement steps from almost the quantum limit in air to 5% in the phantom pictures in Figure 3-14 where, to avoid conventional angiography, a catheter *in situ* provided the calibration data to correct for attenuative differences and Compton spread.

A diagnostic x-ray source with its attendant spatial resolution (about 0.5 mm x 0.5 mm) was used to generate the pencil beam (see Figure 1-1b) results shown in Figure 3-15. The chordal measurements on this 4.67-millimeter diameter tube filled with a dilute solution of contrast agent were corrected using a single-scatter code, IMAGE, that assumes central stacking of slices. Two different concentrations are shown to highlight the effects of self absorption.

Different injection rates and the curve fitting routines described in Appendix C were used to make the flow rate calculations graphed in Figure 3-16. Measurements were performed using the therapeutic x-ray source and with a turbulence inducer emplaced distal to the catheter in a 1/4-inch tube. Table 3-2 shows the calculated diameter compared to the actual diameter for this procedure. Note that the presence of a laminar-flow boundary layer introduced by the flow system is readily observed with this technique, a manifestation of the sensitivity.

Figure 3-14. Thorax phantom measurements. (a) Catheter at depth calibration curve. (b) Fluorescent response from a 6.33 mm tube at an injection/flow rate combination that achieves 2% contrast medium concentration at the imaging site. Note the severe degredation of both signals at either side due to presence of the aluminum rods. (c) Reconstructed diameter measurements versus the actual diameter. Positioning at the edges is thought to have caused the discrepancies.

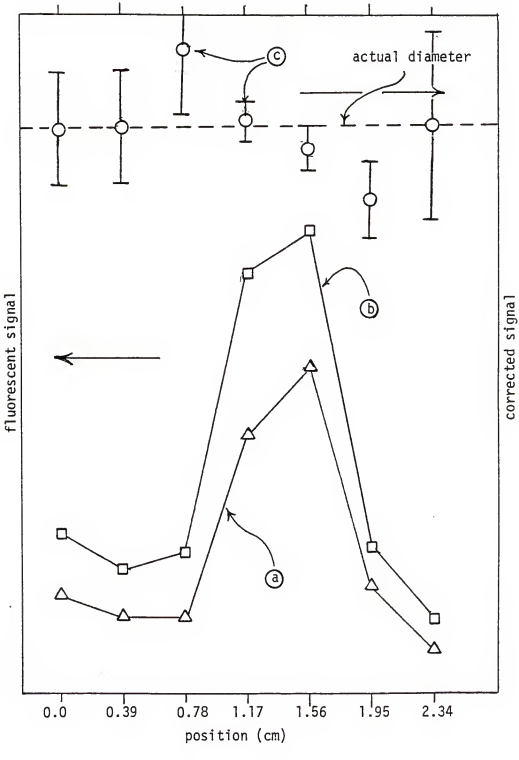
actual diameter
c
b
a
fluorescent signal
corrected signal
0.0
0.39
0.78
1.17
1.56
1.95
2.34
position (cm)

Figure 3-15. Chordal measurements via pencil beam illumination. A 4.67 mm tube with (a) 5% and (b) 15% contrast medium solution. Note the teardrop effect of self attenuation as the optical path becomes significant. (c) the measurements in (b) corrected for self attenuation by using the BASIC program IMAGE.

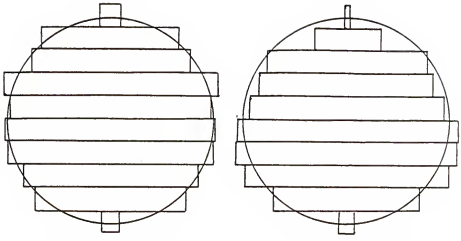

5% concentration 15% concentration

uncorrected

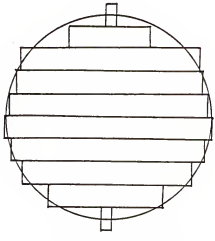

15% concentration

corrected

Figure 3-16. Flow rates measured using fluorescent emission. Parametric least-squares fitting was used to calculate flow rate and cross-sectional area. See Table 3-2.

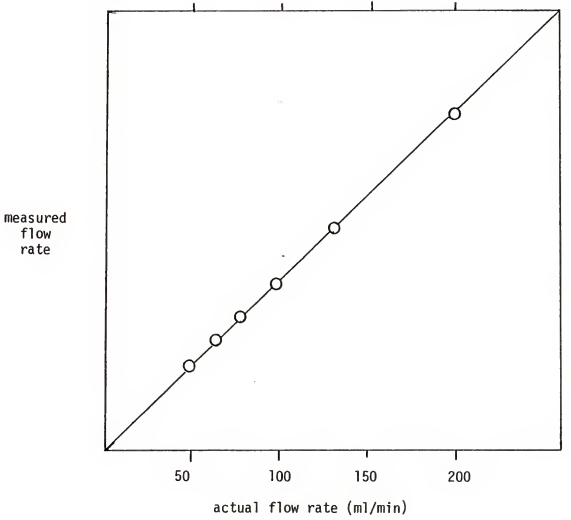
measured
flow
rate
50
100
150
200
actual flow rate (ml/min)

Table 3-2

Flow Parametric Fitting Results on 6.33 mm Diameter Model

Flow Rate (ml/min)	# of Injection Rates	Measured Flow Rate (ml/min)	% Difference	Measured Diameter (mm)	% Difference
192	5	194	+ 1.0	6.18	- 2.4
160	5	163	+ 1.8	6.04	- 4.6
122	5	123	+ .8	6.26	- 1.0
95	5	95.5	+ .5	6.30	- .5
82	5	81.4	- .7	6.44	+ 1.8
60	5	59.0	- 1.6	6.51	+ 2.8

Canine external carotid arteries manually occluded by means of constrictors sited at regular intervals served as an in vivo model. The constrictors were emplaced in the normally 3-millimeter smooth-walled artery so as to create decreasing circular cross-sectional areas along the length of the artery distal to the emplaced catheter. To the extent that the cross sections remained circular the fluorescent emission results could be compared with the results obtained via conventional transmission angiography. By assuming circular cross sections the volumetric results of fluorescence could be reduced to a series of diameters. Conventional angiography diameters were converted to a comparable form by convoluting the measured results with the previously determined point spread function. The comparison illustrated in Figure 3-17 revealed a high degree of correlation ($r = 0.98$) for the two techniques. This was expected considering the circular nature of the lumen pre- and post-occlusion.

The high degree of occlusion compounded with clotting around the inserted "y" drastically reduced the flow rate. Normal flow rates of 150 to 200 ml/min through the artery finally fell below 10 ml/min and could no longer be measured on the electromagnetic flow meter. Subsequently flow rates as low as 3.6 and 0.4 ml/min were measured via fluorescence but could not, of course, be verified.

An inordinate amount of perfusion of contrast agent into the surrounding tissues was noted. This was probably due to the length of the procedure, the low flow rate, the trauma associated with the surgery, and the need to perform conventional angiography. A background subtraction was performed to correct for this effect.

Figure 3-17. Comparison of *in vivo* angiographic measurements using conventional and fluorescent techniques. The canine external carotid was occluded with circular plastic constrictors to vary the cross sections and still retain a valid model for comparison. Rather than scaling the ordinate, the line shown depicts the line along which all the data points should fall assuming that the assumption of circular cross sections is valid.

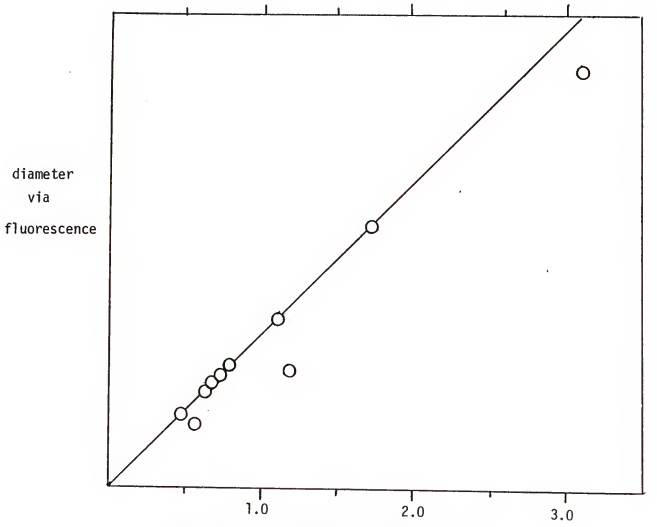
diameter
via
fluorescence
1.0
2.0
3.0
diameter via conventional angiography (mm)

CHAPTER FOUR
DISCUSSION AND CONCLUSIONS

Fluorescent emission imaging can be a useful diagnostic tool. Coupled with the signal reduction methods presented, the fluorescent response of an off-axis detector has been shown to be an effective measure of the cross-sectional area of the arterial lumen. This measure, which is almost completely independent of the angle of incidence and is not subject to observer variability, provides an effective argument for amending conventional transmission angiography. Even replacement, particularly in simple cases where transmural perfusion, pooling, and irrelative motion are not significant problems, may prove feasible. Supportive capabilities for this argument include a significant reduction of invasiveness in terms of contrast agent injected, catheter size inserted, and x-ray dose received. The dose to supporting personnel is significantly lowered. Flow rate past the catheter can be measured.

Normalization

In order to provide a true quantitative measure of the cross sectional area of the lumen some method of determining the normalization constant must be used. The techniques used in this work fall into three categories: a catheter at the imaging site, response of a known circular cross section, and parametric fitting of the response curves. While each method has its advantages, the above listing is generally in decreasing order of reliability and increasing order of non-invasiveness.

Because of its simplicity, using the response of a catheter at the imaging site was most often used to calculate the normalization constant. Appendix E details simple calculations required to establish the detector response on the SAA curve plots. Essentially the technique is to measure the response of a tube in air filled with a known percentage of contrast agent in order to determine geometrical losses and to measure the response of a radiopaque catheter both in air and at depth in order to determine attenuative losses. A simple conversion is then performed to change the attenuation normalization from the elemental constituents of the catheter to that of iodinated contrast agent. Although reliable, this method is by far the most invasive, requiring an object with a known response function to be placed at the imaging site. This poses no problem for angioplastic procedures but for general diagnostic purposes this method is probably unsuitable.

As an adjunct to transmission angiography the calibration can be performed whenever the lumen can be assumed circular and the diameter has been measured via transmission. While this method is locally dependable, during a scan a change in the fluorescent signal in comparison with measured diameter is of indeterminate cause: has the attenuation changed or is the lesion eccentric? Extremely non-invasive in that no catheter must ever be present at the imaging site and only two injections of contrast agent are required to determine both cross-sectional area and flow rate, the drawbacks of requiring transmission angiography and localized certainty of a circular assumption suggest combining this and the third normalizing technique, parametric fitting.

In what has proven to be the most imprecise of the normalization procedures, parametric fitting of the normalization constant via the shape of the response function generated at different injection rates is attractive because of its non-invasive nature--catheterization is not required at the site of measurement and conventional angiography is not required to perform an edge measurement. The need to develop a curve may prove undesirable in that the total amount of contrast as compared to conventional techniques may not be improved, but certainly the lower injection rate contributes to parametric fitting's benign nature. The major problem, however, lies in the relatively large uncertainties in the determination of the normalization constant. It must be remembered that the uncertainties in quantum statistics, the injection rates, the SAA, contrast agent mixing, and fluorescent photon/Compton photon differentiation all contribute to the curve shape. As expected, the fewer the number of parameters determined via least-square-error fitting, the better the results.

No one method, emplaced catheter, conventional measurement, or curve fitting, stands out as best. All three of the normalization techniques work. What must be determined is the acceptable degree of uncertainty in light of the acceptable degree of invasion. As alluded to before, for in vivo work a combination of the latter two methods was found to be most desirable.

Extension of Results

Extrapolation of the results leads to the conclusion that resolution on the order of one millimeter (3% uncertainty, 1/2 second scan) is attainable in the human coronaries given a better (but obtainable) collimation and tracking system. Modern source and

detector systems would easily improve even this resolution of either time or space, or both, by an order of magnitude. This would certainly be sufficient for the diagnosis of heart disease and the tracking of progress during therapy.

While the in vivo validation of flow measurements was impossible, the spectacular results in the tube models suggest the ability to measure flow rate within 2%. Combined with the capacity for using a small catheter, the flow rate--the real gauge of atherosclerotic disease--may be directly quantifiable.

The slant of this work has been coronary angiography because simple x-ray transmission is the best available diagnostic technique. Much peripheral angiography has succumbed to other methods such as ultrasound, nuclear magnetic resonance, and digital subtraction angiography, but fluorescence still has something to offer. Quantifiability, precise location of stenosis, a low degree of invasion, and an accurate flow measurement are difficult to find in any one method.

No other technique promises the speed and precision required to perform laser angioplasty. Since it is possible to simultaneously visualize objects of different materials because the fluorescent peaks occur at different energies, alignment of an optical fiber inside the arterial lumen is observable. The laser pulse used to destroy the stenotic lesion can be triggered after alignment so that the arterial wall is not damaged. Therapeutic results can be precisely tracked via fluorescence.

A Clinical Device

The many advantages of fluorescent emission angiography highlight the need for clinical development. Although equipment exists which

fulfills the requirements for a fluorescent emission system, building a clinical device would require interfacing this equipment to allow enough flexibility to accommodate these advantages. Specific needs can be listed by component.

1. The x-ray source should be stable at high current bursts for long periods of time. The focal spot must be small (less than one millimeter). Fluoroscopy at any angle is an essential feature of the system.

2. The source/collimator and detector/shield systems must be mechanically driven at high speed with high precision.

3. The detector/multichannel analyzer system must be fast (2×10^6 counts/sec) with energy resolvability on the order of a few keV.

4. The injection system must be capable of adjustable, precise injection rates.

5. The computer or computers must serve three purposes: command the collimator, shield, and injection systems; collect information from the image intensifier and the multichannel analyzer; and interpret the data.

Several foreseen clinical complications exist. Perfusion of contrast agent through the arterial wall and into the surrounding tissues, pooling of contrast agent in the beam path, and bending and branching of the arteries loom as obstacles in the useful implementation of fluorescent emission angiography. Conjectural solutions are presented as possible methods of overcoming these problems.

Some transmural perfusion of the contrast agent into the surrounding tissues will occur. The contribution of the perfusion,

however, is thought to be small, at least two to three orders of magnitude reduction in the concentration of iodine in the arterial lumen for a single pass [Mc84]. Such a low percentage allows, for a sufficiently collimated beam, the use of a background subtraction method to eliminate the fluorescent signal from the surrounding tissue. This was the type of correction required in the canine studies in this work after long periods of bolus injection.

If the goal of peripheral injection rather than selective catheterization is to be realized the problem of intercepted blood pools must be addressed. Simple geometric solution appears viable. By choosing an angle of incidence where the coronary ventricles are not illuminated by the incident beam the coronary arteries can be visualized via fluorescence. Of course, the problem of fluorescence due to Compton scatter still exists but manipulating the detector's field of view may prove adequate.

Bending and branching of the arteries is a significant problem especially for coronary arteriography. If it is not possible to insure a projection in which the incident beam is almost perpendicular to the long axis of the artery a false interpretation of the fluorescent signal may result. Note that this same problem occurs in conventional angiography. Bending may be normalized out by using a catheter at depth to calibrate the fluorescent response, branching via inference from the distal and proximal reconstructions. Nevertheless these remain problems that will require some effort to overcome.

Fluorescent emission imaging is no panacea. On the other hand, the potential benefits are enormous. Its speed, precision, and relatively innocuous nature will make it an invaluable tool for the

angiographer. This proof-of-principle work has developed the technical methods and analytical tools to the point of implementation in a clinical device. X-ray fluorescence as an angiographic method is a viable adjunct to current techniques and possibly, in some cases, a replacement.

APPENDIX A
COMPARISON BETWEEN TRANSMISSION AND FLUORESCENCE TECHNIQUES

Consider a beam of photons incident on a thorax model as shown in Figure A-1 in an attempt to measure a 4.67 mm circular-shaped arterial lumen cross section to within 10% quantum uncertainty. The desired resolution is 0.01 cm. The target cross section for transmission angiography and the source volume for fluorescence are also shown in Figure A-1. There are two major differences in the physical parameters of the techniques: for transmission angiography the average photon energy of the x-ray beam is about 45 keV and the contrast agent is about 75% concentration in the vessel while for fluorescent emission angiography the beam energy is about 35 keV and the concentration is 5%.

For the purpose of this analysis a small, $(0.01)^3 cm^3$, volume within the arterial lumen was chosen at the side furthest away from the detector because attenuation within the arterial lumen makes this position particularly difficult to measure via fluorescence. Although its thinness makes this a difficult cross section for conventional angiography, the position at the edge is precisely what the angiographer hopes to measure.

By assuming a reasonable model for attenuation coefficients,

$\bar{\mu}_{35} = .5 + 9p \ [cm^{-1}]$

$\bar{\mu}_{45} = .25 + 4.5p \ [cm^{-1}]$

Figure A-1. A comparison of transmission and fluorescent quantum uncertainties. A beam of x rays is passed through 5 cm of tissue and impinges upon an artery filled with contrast solution. For transmission the average energy is 45 keV and 75% solution; for fluorescence, 35 keV and 5% solution. The transmission beam passes through 15 cm of tissue after being absorbed by the comparative volume (see inset) to hit the film and give I(in), or can just miss the comparative volume to give I(out). Detection schemes compare the difference between I(in) and I(out) to give a measurement uncertainty, $\sqrt{I(in)+I(out)}$ The fluorescent beam hits the comparative volume and a detector 5 cm away senses the iodine-produced photons. The fluorescent measurement uncertainty is $2\sqrt{I(fluor)}$ which in terms of percentage is always less than for transmission angiography. Also shown are the imaged lumina--for fluorescence a true 3-dimensional quantity, for transmission a 2-dimensional projection.

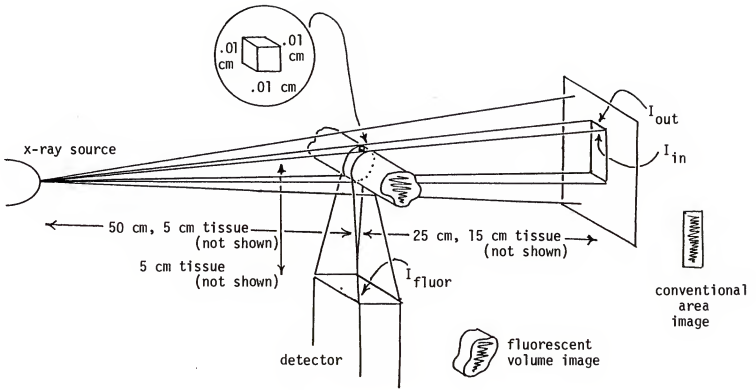
.01 cm
.01 cm
.01 cm
x-ray source
I_{out}
I_{in}
50 cm, 5 cm tissue (not shown)
25 cm, 15 cm tissue (not shown)
5 cm tissue (not shown)
I_{fluor}
conventional area image
detector
fluorescent volume image

$\mu' = .3 + 3.5p \ [cm^{-1}]$

$N\bar{\tau} = 5p = .25 \ [cm^{-1}]$

($\bar{\mu}$,μ', $N\bar{\tau}$ and p are defined as in the Analysis section), one can calculate the transmission current just inside and outside the artery,

$$I^{in}_{trans} = (1.150 \times 10^{-10})I_o \quad [photons/sec]$$

$$I^{out}_{trans} = (1.198 \times 10^{-10})I_o \quad [photons/sec],$$

where I_o is the number of photons output by the machine. To determine the difference between inside and outside the artery a comparison between I_{in} and I_{out} is made, for simplicity assume a perfect detector that subtracts the background, I_{out}, from I_{in}. A ten percent error in this measurement requires 1.019×10^{15} photons to be emitted from the source.

The same number of photons emitted from the x-ray source results in about 4.7 percent quantum error in the number of fluorescent photons detected. This value was derived from the square artery approximation with constant cross section so

$$I_{fluor} = (1.748 \times 10^{-12})I_o \quad [photons/sec]$$

and the assumption that the Compton noise is three times as large as the fluorescence.

Ten percent quantum uncertainty using fluorescent emission requires 1/5 the number of photons and results in about 1/10 the dose of that given in conventional angiography. The required contrast agent percentage is drastically lower. Most importantly, by using fluorescent emission, one gains three-dimensional rather than two-dimensional information about the lumen.

It is obvious that choosing the analyzed volume at the edge closest to the detector would give fluorescence an even greater advantage. If a similar cross section is chosen in the center of the artery, however, the advantage is not so obvious. The advantage of transmission is the exponential decrease of I_{in} as the lumen gets larger while I_{flour} experiences something less than linear growth. Nevertheless, the same sort of analysis performed at the center of the 4.67 mm artery shows that transmission and fluorescence techniques require almost the same number of photons to achieve the same quantum uncertainty. Once again, however, with conventional angiography the observer has obtained an outline of a volume rather than the volume.

Assuming that the dose varies as the square of the kVp in this region and that the field sizes for transmission angiography as compared to fluorescent methods is 20 cm x 20 cm versus 1 cm x 5 cm, the reduction factor, RF, for local and integrated x-ray dose to the patient becomes

$$RF(\text{local}) = (35/45)^2 = .60,$$

$$RF\ (\text{integral}) = (35/45)^2(5/400) = 7.6 \times 10^{-3}.$$

As a first approximation the dose reduction to angiographic personnel can be assumed to be equal to the reduction in integral dose to the patient.

APPENDIX B
THE SQUARE ARTERY APPROXIMATION

As previously stated in the Analysis section, the fluorescent signal from an artery with circular cross section, as shown in Figure 2-1, can be written

$$S = K \int_E N\tau_c\phi_I \int_{-r}^{r} e^{-\mu' y - \mu(r^2-y^2)^{1/2}} \int_{-z_o}^{z_o} e^{-\mu z - \mu'(r^2-z^2)^{1/2}} \, dz dy dE$$

with terms defined as before.

Because this expression is rather unwieldly, it is advantageous to make the assumption that the cross section, rather than being circular, is square. Keeping the cross sectional area constant, so that α, the length of a side on the square, is equal to $\sqrt{\pi}\cdot r$, the spatial integrals can be evaluated to give

$$\begin{aligned} S &= K \int_E N\tau_c\phi_I \int_{-\alpha/2}^{\alpha/2} e^{-(z+\alpha/2)} \int_{-\alpha/2}^{\alpha/2} e^{-\mu'(y+\alpha/2)} dy dz dE \\ &= K \int_E N\tau_c\phi_I \left(\frac{1-e^{-\mu\alpha}}{\mu}\right)\left(\frac{1-e^{-\mu'\alpha}}{\mu'}\right) dE \\ &= K \frac{1-e^{-\mu'\alpha}}{\mu'} \int_E N\tau_c\phi_I \frac{1-e^{-\mu\alpha}}{\mu} \, dE \quad . \end{aligned}$$

Assuming a small spectral change as the beam passes through the artery allows the spectral weighting of the photoelectric cross section and the linear attenuation coefficient to give $\bar{\tau}_c$ and $\bar{\mu}$, respectively. The resultant expression is termed the square artery approximation

[SAA] and has been shown in the text to be a valid model when the total optical path length, $\bar{\mu}\alpha + \mu'\alpha$, is less than one.

APPENDIX C
LEAST SQUARES FITTING PROCEDURE FOR
MULTIPLE INJECTION RATES

Despite the injection rate, the only conditions for validity of the square artery approximation are thorough mixing and a small (less than one optical path length) concentration of contrast agent. Then, for a series of injections, the signal from the i^{th} injection may be written

$$S_i = Kp_i \, Q_i' \, \overline{Q}_i$$

where K is a constant of proportionality to include attenuative and geometrical effects and the other terms are defined as follows:

p_i is the percent contrast agent in the artery given by $p_i = I_i/I_i+F$.

$Q_i' = (1-e^{-\mu_i'\alpha})/\mu_i'$ and

$\overline{Q}_i = (1-e^{-\overline{\mu}_i\alpha})/\overline{\mu}_i$

where $\alpha = \sqrt{\pi \cdot r}$ for a circular cross section

and

$$\mu_i' = \gamma' p_i + \delta'$$

and

$$\overline{\mu}_i = \overline{\gamma} p_i + \overline{\delta}$$

with $\gamma', \delta', \overline{\gamma}$ and $\overline{\delta}$ previously defined.

Given a series of data points the total square error, ε^2, may be written

$$\varepsilon^2 = \sum_i [S - kpQ'\bar{Q}]^2 = \sum_i (S - K\beta)^2$$

where the subscripts have been dropped for convenience.

The least squares fitting method requires finding the minimum point on the multidimensional surface described by $\varepsilon^2(\alpha, F, K, \ldots)$. This is accomplished by finding the point where the first derivatives of the number of parameters desired to span the space vanish (e.g., $\partial\varepsilon^2/\partial x = 0$; $\partial\varepsilon^2/\partial F = 0$). An iterative method of solution is used whereby an initial guess must be made. Because of the non-linear nature of the error function this guess must be close enough to assure convergence of the solution to the minimum. This initial guess is rarely a problem due to the constraints of the physical or biological system.

Iterative steps are made by calculating the second derivatives and adjusting via the formula,

correction = - (first derivative)/(second derivative).

Although this method does not assure convergence, tracking the calculated error, ε^2, also tracks the convergence of the selected parameters within the chosen bounds. Finding a point of non-convergence, within the truncation error introduced by the microcomputer, is extremely rare and can be circumvented by choosing a different starting value.

Parameters fitted using this technique included

α, the length of the side of the square in the SAA,

F, the flow rate,

K, the normalizing constant resulting from geometric and attenuation effects as well as Compton spread, and

B, the background signal from iodine diffusion into the surrounding tissues.

The formulas of first and second derivatives, with the exception of those with respect to background, are shown below because the included algebra is somewhat tedious (equations C-1 through C-6).

$$\frac{\partial \epsilon^2}{\partial \alpha} = \sum_i 2K(K\beta - S)\beta_\alpha \qquad \text{(C-1)}$$

where $\beta_\alpha = p(Q'_\alpha \overline{Q} + Q' \overline{Q}_\alpha)$

where $Q'_\alpha = e^{-\mu' \alpha}$ and $\overline{Q}_\alpha = e^{-\overline{\mu}\alpha}$.

$$\frac{\partial^2 \epsilon^2}{\partial \epsilon^2} = \sum_i 2K[K\beta_\alpha^2 + (K\beta - S)\beta_{\alpha 2}] \qquad \text{(C-2)}$$

where

$$\beta_{\alpha 2} = p[2\overline{Q}_\alpha Q'_\alpha - \mu' Q'_\alpha - \overline{\mu} \overline{Q}_\alpha] \ .$$

$$\frac{\partial \epsilon^2}{\partial F} = \sum_i 2K(K\beta - S)\beta_F \qquad \text{(C-3)}$$

where $\beta_F = \beta_p p_F$

with $p_F = -\frac{I}{(I+F)^2}$

and $\beta_p = \overline{Q}\, Q' + p\overline{Q}\, Q' + pQ'\overline{Q}_p$

where $Q'_p = \gamma' Q'_\mu = \gamma' \left(\frac{\alpha e^{-\mu\alpha} + Q'}{\mu'} \right)$

and $\overline{Q}_p = \overline{\gamma Q}_\mu = \overline{\gamma} \left(\frac{\alpha e^{-\overline{\mu}\alpha} + \overline{Q}}{\overline{\mu}} \right)$.

$$\frac{\partial^2 \varepsilon^2}{\partial F^2} = \sum_i 2K[K\beta_F{}^2 + (K\beta - S)\beta_{F2}] \qquad \text{(C-4)}$$

where $\beta_{F2} = \beta_{p2}\ p_F{}^2 + \beta_p p_{F2}$

where $p_F = \frac{2I}{(I+F)^3}$

and $\beta_p = 2\bar{Q}_p Q' + 2Q_p'\bar{Q} + 2pQ_p'\bar{Q}_p + p\ (\bar{Q}\ Q_p' + Q'\bar{Q}_p)$

where

$$Q_p' = -\frac{(\gamma')^2}{\mu'}\ (\alpha^2 e^{-\mu'\alpha} + 2Q'_\mu)$$

and $\bar{Q}_{p2} = -\frac{\bar{\gamma}^2}{\bar{\mu}}(\alpha^2 e^{-\bar{\mu}\alpha} + 2\bar{Q}_{\bar{\mu}})$.

$$\frac{\partial \varepsilon^2}{\partial K} = \sum_i (-2\beta(S - K\beta)) \quad . \qquad \text{(C-5)}$$

$$\frac{\partial^2 \varepsilon^2}{\partial K^2} = \sum_i 2\beta^2 \quad . \qquad \text{(C-6)}$$

APPENDIX D
COMPUTER PROGRAMS

Extensive use of the computer as an analytical tool and as an efficient method of data collection and reduction facilitated this work. Rather than list the actual programs, a brief synopsis of the function and methods which proved useful and is presented here. Only those programs that have general applicability and would be useful in continuing this work are discussed.

Two computers were used in the analytical section. Programs coded in FORTRAN were run on a PDP 11/34.® BASIC programs were run on a Commodore-64® microcomputer. This same microcomputer interfaced with the multichannel analyzer to collect data and reduced the results using the analytical tools developed.

Analytical Programs

CSIG (FORTRAN) calculates the fluorescent signal from any shape lumen and stenosis due to Compton scatter from five centimeters of ingress and five centimeters of egress tissue. This is a worst-case calculation in that solid angle calculations assume a full artery lumen or either side of the two-dimensional cross section. CSIG was used to study the contribution of false signal due to Compton-scattered x rays. With the exception of the first Compton scatter, single scatter is assumed.

FLUOR (BASIC) performs a single point, $(.01)^3 cm^3$, fluorescence calculation at depth. Attenuation of incident and exiting beams

through varying quantities of tissue adjusts the input spectrum and fluence as well as the output fluence. Energy and space are discretized. FLUOR is used in conjunction with NOISE to determine relative numbers of fluorescence and Compton photons at the detector.

FSIG (FORTRAN) determines the fluorescent signal from any shape arterial lumen. Corrections for attenuation of the signal in and out is made via single-scatter analysis. Cross sections are calculated based upon water and a user-chosen percentage of Renografin-76®. Discretized quantities include space and energy--$(.01)^3 cm^3$ and 1 keV, respectively. Tabulated results are output by .01 cm slice.

NOISE (BASIC) calculates the Compton photons that reach the detector as a beam is passed through tissue. The code allows the user to shield the detector so as to narrow the Compton source volume as is done physically. Peak-to-Compton ratios were determined with NOISE and FLUOR.

PHOTRANS (FORTRAN) is a three-dimensional Monte Carlo transport code that samples the incident flux, the cross-sectional data, and the Klein-Nishina relation to determine the detector response from any size circular lumen without attenuation from surrounding tissue. Cross sections are calculated based upon a prompted contrast-agent percentage diluted in water. Although spatial weighting and Russian roulette were used to reduce particle histories, the time consuming nature of this method limited the use of PHOTRANS to verification of curve shapes. Random numbers were generated via a multiplicative congruential method.

Data Collection, Reduction, and Display

DIFF/FOUR (BASIC) takes the differential of a curve generated by

a series of data points to give the one-dimensional point spread function. The coefficients of a sine/cosine series fit are then calculated to give the expansion in Fourier space. Data and functions are plotted to verify the validity of the method.

FILE PICT (BASIC) generates a three-dimensional picture of an arterial lumen from a series of responses due to fan-beam fluorescence assuming circular cross sections. While calibration can be achieved via either a catheter signal at depth or different injection rate responses, a strict linearity assumption makes this program realistically useful only with an at-depth catheter calibration. The square artery assumption is used to correct for self absorption.

FIT ALL (BASIC) can be used to fit the normalization constant, the size parameter (the square root of the cross-sectional area), the flow rate, and/or the background signal for a series of data points generated from different injection rates at the same imaging location. The SAA models the fluorescent response. The method is described in Appendix C.

GET LOOP (BASIC) is the interface program designed to retrieve spectral data from the multichannel analyzer. Retrieval, interpretation, and storage requires about five minutes per 256-channel spectrum.

IMAGE (BASIC) assumes central stacking of slices to create a cross sectional picture of the arterial lumen from detector response to a pencil beam of x rays swept perpendicularly through the artery. Building from the bottom up, an iterative process uses single scatter to determine the size of next upper slice considering the shape of lumen between the illuminated slice and the detector.

PEAK LOOP (BASIC) analyzes a series of spectra to separate fluorescent peaks from Compton scatter. Location of the fluorescent signal is user-determined and input via PLOT SPECT. Second-order polynomial least squares fitting is used to determine the Compton contribution in the fluorescence channels. K_α and K_β peaks are separated by means of integral determination in distinguishable channels.

PLOT SPECT (BASIC) permits the user to select the limits of fluorescent peak channels via a cursor tracked along the detector spectrum displayed on the terminal. Multiple peaks may be selected and stored. The output file of PLOT SPECT is used in PEAK LOOP to select the channels for analysis.

PRINT FILE (BASIC) is used to print a standard format peak file.

READ FILE (BASIC) prints the standard format peak files to the display monitor.

REALSIG (BASIC) folds the point spread function determined using DIFF/FOUR into a series of actual diameters to give the response in convolution space. Interpolation is via a Fourier series expansion.

SIMPLE PICT (BASIC) displays, as a three-dimensional picture, lumen cross-sectional data assuming circular sections. This program is a graphic tool used in studies that depend on injection rate curves to determine cross-sectional area.

WEIGHTAVELOOP (BASIC) calculates flux weighted cross sections for different percentages of contrast agent diluted in water. From this program, the simple linear dependence of $\bar{\mu}$, μ' and $\bar{\tau}$ was verified.

APPENDIX E
CALCULATION OF THE NORMALIZATION CONSTANT USING A CATHETER AT DEPTH

Because the fluorescent signal changes drastically with changes in either the geometry or in the attenuative materials in the ingress and egress x-ray paths, a calibration is required to locate the response on the SAA curves. As mentioned in the main text, the most straightforward method requires three measurements:

1. The fluorescent response of the detector due to a known cross-sectional area tube with a known concentration of iodine, S_{air}^{tube}.

2. The fluorescent response of an opaque catheter at the same location in air, S_{air}^{cath}.

3. The fluorescent response of the same catheter at the same geometric location (if impossible, r^2 changes can be calculated) at depth in the tissue, S_{tissue}^{cath}.

The normalization factor for geometrical effects may be written

$$K_g = N\tau_c \frac{(1-e^{-\bar{\mu}\alpha})\,(1-e^{-\mu'\alpha})}{\bar{\mu}\,\mu'} / S_{air}^{tube}$$

where $N\bar{\tau}$, $\bar{\mu}$, μ', and α are calculated for the calibration tube.

For a catheter with iodine as the absorber the attenuation portion of the normalization constant reduces to

$$K_a = S^{cath}_{tissue} / S^{cath}_{air}$$

A problem occurs when the catheter uses an element other than iodine to achieve its opacity. All of the catheters used in this work had a pronounced tin peak upon which the calibration was performed. By assuming the attenuative corrections can be modeled by $K_a^I = e^{-\mu(Water,I)x}$ and $K_a^{Sn} = e^{-\mu(Water,\ Sn)x}$ (although this is not strictly true in the case of the incoming beam it serves here as a good first order approximation) one can solve for

$$K_a^I = \left(K_a^{Sn}\right)^{\mu(Water,\ 28.5)/\mu(Water,\ 25.1)}$$

or

$$K_a^I = \left(K_a^{Sn}\right)^{.79}$$

REFERENCES

Ah81 Ahlgren, L. and S. Mattsson (1981) Cadmium in man measured in vivo by x-ray fluorescence analysis Phys. Med. Biol. 26(1):19-26.

Bi79 Birch, R., Marshall, M. and Ardran, G. M. (1979) Catalogue of Spectral Data for Diagnostic X Rays. Physicists Association, Reedprint, Great Britain.

Br83 Brown, B.G. (1983) Arteriographic assessment of coronary disease advantages, limitations and clinical uses of a computer assisted method Cardiology Update, 1983 Edition. Rapaport, E. (ed), Elsevier Biomedical, New York pp. 67-98.

Ca76 Carter, L.L. and E. D. Cashwell (1976) Particle Transport Simulation with the Monte Carlo Method, ERDA Critical Review Series, USERDA Technical Information Center, Oak Ridge, Tennessee.

Co80 Committee on the Care and Use of Laboratory Animals of the Institute of Laboratory Animal Resources, National Research Council, U.S. Department of Health Education and Welfare, Public Health Service, NIH, (1980) Guide for the Care and Use of Laboratory Animals, NIH Publication 80-23 Washington, D.C.

Gr72 Grubb, R.L. Jr., Phelps, M.E. and Ter-Pogossian, M.M. (1972) Regional cerebral blood volume in humans Arch. Neurol 28:38-44.

Ho71 Hoffer, P.B., Gottschalk, A., and Foster J. (1971) Fluorescent thyroid scanning Radiology 99:117-123.

Ho73 Hoffer, P.B., Gottschalk, A., and Foster J. (1973) Excitation thyroid laminography theoretical and practical considerations Tomographic Imaging in Nuclear Medicine, Freedman, G.S. (ed), New York Society of Nuclear Medicine, New York pp. 57-65.

Ho68 Hoffer, P.B., Jones, W.B., Crawford, R.B., Beck, R.N. and Gottschalk, A. (1968) Fluorescent thyroid scanning a new method of imaging the thyroid Radiology 90:342-344.

Hu69 Hubbell, J.H. (1969) Photon cross sections, attenuation coefficients, and energy absorption coefficients from 10 keV to 100 GeV., NSRDS-NBS 29, Washington, D.C.

Hu75 Hubbell, J. H., Viegele, W. J., Briggs, E.A., Brown, R. T., Cromer, R. T. and Howerton, R. J. (1975) Atomic form factors, incoherent scattering functions, and photon scattering cross sections, Journal of Physical and Chemical Reference Data, 4:3 American Chemical Society and the American Institute of Physics.

Ka72 Kaufman, L., Shames, D. M., Greenspan, R. H., Powell, M. R., and Perez-Mendez, V. (1972) Cardiac output determination by fluorescence excitation in the dog Invest. Radiol. 7:365.

Ka73 Kaufman, L., Shames, D. M., Greenspan, R. H., Powell, M. R., and Perez-Mendez, V. (1973) A new method of measuring cardiac output using fluorescent emission Semiconductor Detectors in Medicine USAEC Office of Information Services Technical Information Center, Washington, D.C. p. 353-364.

Ko76 Koehler, R.E., Kaufman, L. and Brito, A. (1976) In vivo measurement of hepatic iodine concentration using fluorescent excitation analysis Invest. Radiol. 11:134-137.

Kr81 Kruger, R. A. (1981) Estimation of the diameter of and iodine concentration within blood vessels using digital radiography devices Med. Phys. 8:652.

Mc84 McInerney, J. J. (1984) Division of Cardiology, Milton S. Hershey Medical Center, Pennsylvania State University, personal communication.

Ni84 Nichols, A.B. Gabriele, C. F. O., Fenozlio, J. J., Jr., and Esser, P.D. (1984) Quantification of relative coronary arterial stenosis by cinevideodensitometric analysis of coronary arteriograms Circulation 69:512.

Pa76 Patton, J.A., Hollifield, J.W., and Brill, A.B. (1976) Differentiation between malignant and benign solitary thyroid nodules by fluorescent scanning J. Nucl. Med. 17:17-21.

Sq82 Squibb Radiology Reference (1982) ER Squibb and Sons, Inc., Princeton, New Jersey.

St61 Strain, W.H. and S. M. Rogoff (1961) The radiopaque media: nomenclature and chemical formulas Angiography, H. L. Abrams (ed), Little, Brown, and Company, Boston, pp. 35-62.

Te72 Ter-Pogossian, M.M., Phelps, M.E., Grubb, R.L., Jr., and Gado, M. (1971/1972) Measure of regional cerebral blood volume in vivo by means of stimulated x-ray fluorescence, and factors affecting this parameter Europ. Neurol. 6:218-223.

Te71 Ter-Pogossian, M.M., Phelps, M.E., and Lassen, M. (1971) In vivo measure of regional cerebral blood flow and volume by means of x-ray fluorescence Part A - Methodology; Phelps, M.E., Ter-Pogossian, M.M., and Hecht, J. (eds) Part B - Instrumentation in Semiconductor Detectors in the Future of Nuclear Medicine, Hoffer, P.B., Beck, R.N., and Gottschalk, A. (eds) New York Society of Nuclear Medicine Inc. pp. 240-257.

Th78 Thrall, J.H., Gillen, M.T. and Johnson, M.C. (1978) Quantitative thyroid fluorescent scanning: technique and clinical experience Am J. Roentgenol 130:517-522.

Zi76 Zir, L. M., Miller, S. W., Dinsmore, R. E., Gilbert, J. P., and Hawthorne, J. W. (1976) Inter-observer variability in coronary angiography Circulation 53:627.

BIOGRAPHICAL SKETCH

William S. Bice, Jr., is the son of a retired U.S. Army Colonel, William, and an ex-Army nurse, Patricia. Born in 1951 in El Paso, Texas, he has lived in many places in the United States, Europe and the Far East. After graduation from the United States Military Academy at West Point, New York, in 1973, he was commissioned as an officer in the regular Army. Later that year he married Patrice C. Dahle, herself the child of an Army family. Interspersed with tours as an Engineer Officer, William received a Master of Science degree in physics from the University of Illinois in 1977. In 1982 he was chosen under the long-term civilian training program to attend the University of Florida to pursue a Doctor of Philosophy degree with emphasis on medical physics. Major and Mrs. Bice have three sons, William (6), Gregory (4), and Thomas (2).

I certify that I have read this study and that in my opinion it conforms to acceptable standards of scholarly presentation and is fully adequate, in scope and quality, as a dissertation for the degree of Doctor of Philosophy.

Alan M. Jacobs, Chairman
Professor of Nuclear Engineering Sciences

I certify that I have read this study and that in my opinion it conforms to acceptable standards of scholarly presentation and is fully adequate, in scope and quality, as a dissertation for the degree of Doctor of Philosophy.

Carl J. Pepine
Professor of Medicine

I certify that I have read this study and that in my opinion it conforms to acceptable standards of scholarly presentation and is fully adequate, in scope and quality, as a dissertation for the degree of Doctor of Philosophy.

Edward E. Carroll
Professor of Nuclear Engineering Sciences

I certify that I have read this study and that in my opinion it conforms to acceptable standards of scholarly presentation and is fully adequate, in scope and quality, as a dissertation for the degree of Doctor of Philosophy.

Stephen H. Curry
Professor of Pharmacy

I certify that I have read this study and that in my opinion it conforms to acceptable standards of scholarly presentation and is fully adequate, in scope and quality, as a dissertation for the degree of Doctor of Philosophy.

John Staudhammer
Professor of Electrical Engineering

I certify that I have read this study and that in my opinion it conforms to acceptable standards of scholarly presentation and is fully adequate, in scope and quality, as a dissertation for the degree of Doctor of Philosophy.

George R. Dalton
Professor of Nuclear Engineering Sciences

This dissertation was submitted to the Graduate Faculty of the College of Engineering and to the Graduate School and was accepted as partial fulfillment of the requirements for the degree of Doctor of Philosophy.

August, 1985

Dean, College of Engineering

Dean, Graduate School